atoms

MDPI

Article

$Al_2C_4H_2$ Isomers with the Planar Tetracoordinate Carbon (ptC)/Aluminum (ptAl)

Abdul Hamid Malhan [1], Sony Sobinson [1], Nisha Job [1], Shilpa Shajan [1], Surya Prakash Mohanty [1], Venkatesan S. Thimmakondu [2] and Krishnan Thirumoorthy [1,*]

[1] Department of Chemistry, School of Advanced Sciences, Vellore Institute of Technology, Vellore 632 014, Tamil Nadu, India
[2] Department of Chemistry and Biochemistry, San Diego State University, San Diego, CA 92182-1030, USA
* Correspondence: thirumoorthy.krishnan@vit.ac.in

Abstract: Forty-one isomers of $Al_2C_4H_2$ that lie within 50 kcal mol^{-1} are theoretically identified in this work using density functional theory. Among these, isomers **3** and **14** contain a planar tetracoordinate carbon (ptC) atom that lies at 3.3 and 16.9 kcal mol^{-1}, respectively, and are above the global minimum geometry **1** at the ωB97XD/6-311++G(2d,2p) level of theory. The other ten isomers that also contain unique bonding features are isomers **4**, **18**, **20**, **21**, **22**, **27**, **28**, **31**, **34**, and **40**. Out of these isomers, **4**, **18**, **20**, **22**, **27**, **28**, and **34** contain planar tetracoordinate aluminum (ptAl) whereas isomers **31** and **40** contain both ptC and ptAl atoms. Chemical bonding characteristic features are thoroughly analyzed for all these eleven isomers with various bonding and topological quantum chemical tools, such as NBO, AdNDP, WBI, and ELF, except isomer **27** due to the observed elongated Al-Al bond length. The current results indicate that ptC isomer **3** is more stable than other isomers because electron delocalization is more prevalent and it also has double aromaticity as observed from the ELF, NICS, and AdNDP analysis. Further, the structural stability of these isomers is investigated through ab initio molecular dynamics (AIMD) simulation. Isomer **21** shows the planar pentacoordinate aluminum but it is observed as a kinetically unstable geometry from AIMD and, further, one could notice that it isomerizes to isomer **12**.

Keywords: $Al_2C_4H_2$; planar tetracoordinate carbon; planar tetracoordinate aluminum; delocalization; anti-van't Hoff–Le Bel; computational chemistry

Citation: Malhan, A.H.; Sobinson, S.; Job, N.; Shajan, S.; Mohanty, S.P.; Thimmakondu, V.S.; Thirumoorthy, K. $Al_2C_4H_2$ Isomers with the Planar Tetracoordinate Carbon (ptC)/Aluminum (ptAl). *Atoms* **2022**, *10*, 112. https://doi.org/10.3390/atoms10040112

Academic Editor: Alexander Alijah

Received: 2 September 2022
Accepted: 8 October 2022
Published: 11 October 2022

1. Introduction

Planar tetracoordinate carbon (ptC) has made tremendous progress in the past five decades both theoretically [1–10] and experimentally [11–20]. This concept is a fundamental deviation from the conventional ideas of tetrahedral tetracoordinate carbon, which was independently postulated by van't Hoff and Le Bel in 1874 [18,21,22]. For a century, van't Hoff and Le Bel's tetrahedral carbon model went unchallenged. Later, computational predictions and experimental observations led to the initial discovery of planar tetracoordinate or hypercoordinate compounds [4,23]. In 1968, H. J. Monkhorst first proposed the idea of ptC as a transition state for a non-dissociative racemization process [24]. Two years later, in 1970, Hoffmann et al. proposed two ways to stabilize ptC, which have served as a basic guideline for the design of ptC species [25] to date. First, the mechanical strategy was employed with transition metals, conjugative rings, or cages to induce the formation of ptC. On the other hand, the electronic strategy involved using strong σ-donor and π-acceptor ligands or aromatic delocalization to stabilize the lone pair present in the p-orbital on the ptC center. Based on the latter strategy, Schleyer and coworkers theoretically identified the first set of ptC molecules in 1976 but they were not global minimum geometries [26]. Since then, the chemistry of ptC has been extensively studied both theoretically and experimentally as well. Further, it has been extended to planar hypercoordinate carbon (phC) [4,27]

as well as nanosized systems [28–31]. These ptC molecules not only challenge our current understanding of "chemical bonding," but also have potential applications in materials science [31,32].

Only a few ptC compounds, either global or local minimum energy structures, have been experimentally identified to date [13,15,16,33] and other ptC molecules are elusive in the laboratory to date. In this direction, the identification of a ptC structure for a particular elemental composition leads to a high chance of theoretical viability and it delineates a new path to synthetic feasibility [16,33–38]. Dong et al. and Zhang et al. experimentally achieved the ptC clusters of C_2Al_4 [37] and C_5Al_5 [39], respectively, and were predicted to be the global minimum theoretically [40,41]. These two outstanding experimental achievements on aluminum clusters demonstrated that ptC structures are substantially feasible in the experimental laboratory.

Clusters of aluminum and carbon atoms have attracted a lot of attention because they can form non-classical and non-stoichiometric structures [4,42–44] different from most other metal carbide clusters with the cubic framework or layered structures. In 2022, Zhang and co-workers explored them both theoretically and experimentally and identified the most stable structure containing ptC in the carbon-doped aluminum clusters Al_nC^- (n = 6–5) [45]. In the past, Naumkin explored the flat structural motifs of small alumino-carbon clusters C_nAl_m (n = 2–3, m = 2–8) and identified unique clusters featuring ptC and phC [46]. Wu and co-workers identified the global minimum geometry of simple aluminum carbon clusters containing two ptCs [40]. Das et al. identified the global minimum ptC geometries of $CSiGaAl_2^{-/0}$ and $CGeGaAl_2^{-/0}$ systems, exhibiting both σ and π aromaticity [47].

The aluminum and carbon-based molecules could be used in cluster assembled materials [7,9], energy storage [48], aluminum nanoparticle protection, and two-dimensional donor materials in solar cells [49]. In 2021, the global minimum structures of aluminum-bearing planar tetracoordinate carbon isomers of $CAl_4Mg^{0/-}$ [50] and planar tetracoordinate boron, as well as planar pentacoordinate boron isomers of $BAl4Mg^{-/0/+}$ [51], were also reported. Dong et al. synthesized Al_2CH_3, $Al_2C_3H_3$, $Al_3C_3H_2$, $Al_3C_4H_2$, Al_4C_3H, and Al_4C_4H clusters which have hydrogen storage properties [37]. Due to their ability to retain hydrogen and yield combustion products with minimal environmental impact, aluminum clusters have been the subject of several aspects of energy conversion materials development [8,52]. As said above, the exploration of aluminum, carbon, and hydrogen clusters with various molecular chemical compositions has been carried out in the recent past in both theoretical and experimental aspects and their potential applications have also been reported. Meanwhile, a lot of non-classical structure identification has also been carried out in this direction. They may have future potential as alternative fuel resources for overcoming one of the key challenges in developing a hydrogen economy [48] which is in line with one of the 17 UN Sustainable Development Goals [53]. Aluminum carbon clusters containing ptCs have moderate band gaps with wide applications in the areas of semiconductors, optoelectronics, and photovoltaics [28,49]. Al-doped carbon nanotubes have gained a lot of interest because of their nanocatalytic activity in reducing N_2 to NH_3 [54]. Al-doped single-walled carbon nanotubes are superior materials as sensors to detect air pollutants such as CO, NH_3, NO_2, and SO_2 [55,56]. From this point of view, the $Al_2C_4H_2$ system has yet to be explored in detail, hence the present work demonstrates its importance in this field.

On the other hand, aluminum has also been touted as having a significant potential for astrochemical interest [57]. Aluminum is a generously available metallic element in the interstellar medium (ISM) that has a cosmic abundance of$\sim 3 \times 10^{-6}$ [58]. AlCl [59,60], AlF [59,61,62], AlNC [63–65], AlO [66,67], and AlOH [62] are aluminum-bearing molecules that have been detected in the ISM. The depletion of aluminum in interstellar space due to the formation of interstellar dust was well reported [68] and the existence of aluminum in interstellar space is reported as carbonaceous grains [69]. From this point of view, the present work aimed to explore the possible isomers of the $Al_2C_4H_2$ system theoretically

and, in particular, the main focus is given to isomers that have ptC and ptAl isomers lying within 50 kcal mol^{-1}.

2. Computational Methodology

The initial geometries of $Al_2C_4H_2$ isomers are generated by chemical intuition. Density functional theory (DFT) was used to optimize the different possible geometries of $Al_2C_4H_2$ isomers at the B3LYP/6-311++G(2d,2p) [70–73] and ωB97XD/6-311++G(2d,2p) [70,71,74] level of theoretical methods. All the investigated $Al_2C_4H_2$ isomers considered here correspond to the singlet spin state. Harmonic vibrational frequencies are calculated for all the energy minimized geometries to ensure the stationary point on the potential energy surface is a minimum, a transition state, or a higher-order saddle point. Natural bond order (NBO) analysis [75], adaptive natural density partitioning (AdNDP) analysis [76,77], and Wiberg bond indices (WBIs) [78] were used to examine the nature of chemical bonding in the planar tetracoordinate isomers at the ωB97XD/6-311++G(2d,2p) level of theory. Nucleus-independent chemical shift (NICS) values were calculated to measure the π/σ dual aromaticity in isomer **3** [79]. Topological analysis of the electron localization function (ELF) [80] was carried out for the planar tetracoordinate isomers using the Multiwfn program [81]. The ab initio molecular dynamics (AIMD) simulation using the atom-centered density matrix propagation (ADMP) [82] method was performed for the planar tetracoordinate isomers to check their kinetic stability at the ωB97XD/6-311++G(2d,2p) level of theory. In-house Python code was used to generate other possible atomic re-arrangements in the isomers of **1**, **2**, **3**, **4**, **20**, **22**, and **40**. All of these DFT calculations were carried out with the Gaussian suite of programs [83].

3. Results and Discussion

The optimized geometries of $Al_2C_4H_2$ isomers that lie within 50 kcal mol^{-1} at the ωB97XD/6-311++G(2d,2p) level of theory are shown in Figure 1 and their total energy, ZPVE, and ZPVE corrected relative energies are listed out in Table S1. The B3LYP/6-311++G(2d,2p) level of theoretical results is provided in Table S2. Isomer **1** is a global minimum on the potential energy surface with a bent structure. Among these geometries, isomers **3**, **4**, **14**, **18**, **20**, **22**, **27**, **28**, **31**, **34**, and **40** are showing planar tetracoordinate structures that lie at 3.3, 4.3, 16.9, 21.3, 22.9, 24.6, 30.2, 30.9, 34.7, 40.0, and 49.6 kcal mol^{-1}, respectively. Planar pentacoordinate aluminum (ppAl) is observed in isomer **21** which lies at 23.1 kcal mol^{-1} above isomer **1**. All these planar tetracoordinate and pentacoordinate geometries with their bond lengths are shown in Figure 2. Among these, eleven isomers are local minima with zero imaginary frequencies except isomer **40**, which is a first-order saddle point (transition state). Among all the isomers, only two isomers, **3** and **14**, contain a ptC atom, while the other isomers such as **4**, **18**, **20**, **22**, **27**, **28**, and **34** contain ptAl. Isomers **3** and **4** have two planar tetracoordinate centers each. Isomer **3** contains two ptCs whereas isomer **4** contains two ptAls. Three planar tetracoordinate centers are present in isomers **31** and **40**. In contrast to isomer **31**, which has two ptCs and a ptAl, isomer **40** contains two ptAls and a ptC. Even though isomer **27** contains a ptAl center, because of the elongated Al-Al bond length of 3.10 Å, it is excluded from the bonding studies.

3.1. Wiberg Bond Indices

The Wiberg bond indices (WBIs) of isomers **3**, **4**, **14**, **18**, **20**, **21**, **22**, **28**, **31**, **34**, and **40** are shown in Figure 3, which are the measure of electronic parameters related to electron population overlap between two atoms. It indicates the bond order and the characteristic bonding features of these isomers. In isomer **3**, the WBI values for C1–C3, C1–C4, and C2–C4 (numbering scheme followed as shown in Figure 3) are 2.02, 1.22, and 2.02, respectively, which indicates resonance stabilization with alternate double bonds along ptCs. Among the four bonds of the ptC in isomers **14**, **31**, and **40**, one of the bonds has a WBI value close to or greater than two which indicates the π bonds between them. The ppAl–Al bond in isomer **21** has a WBI value of 0.07 which indicates the interaction between them is

electrostatic, but all four C–ppAl bonds have WBI values in the range of 0.36 to 0.76 which indicates the single bonds between them. In contrast to isomers with ptAl, which only have four σ bonds, isomers with ptC have one π bond and four σ bonds.

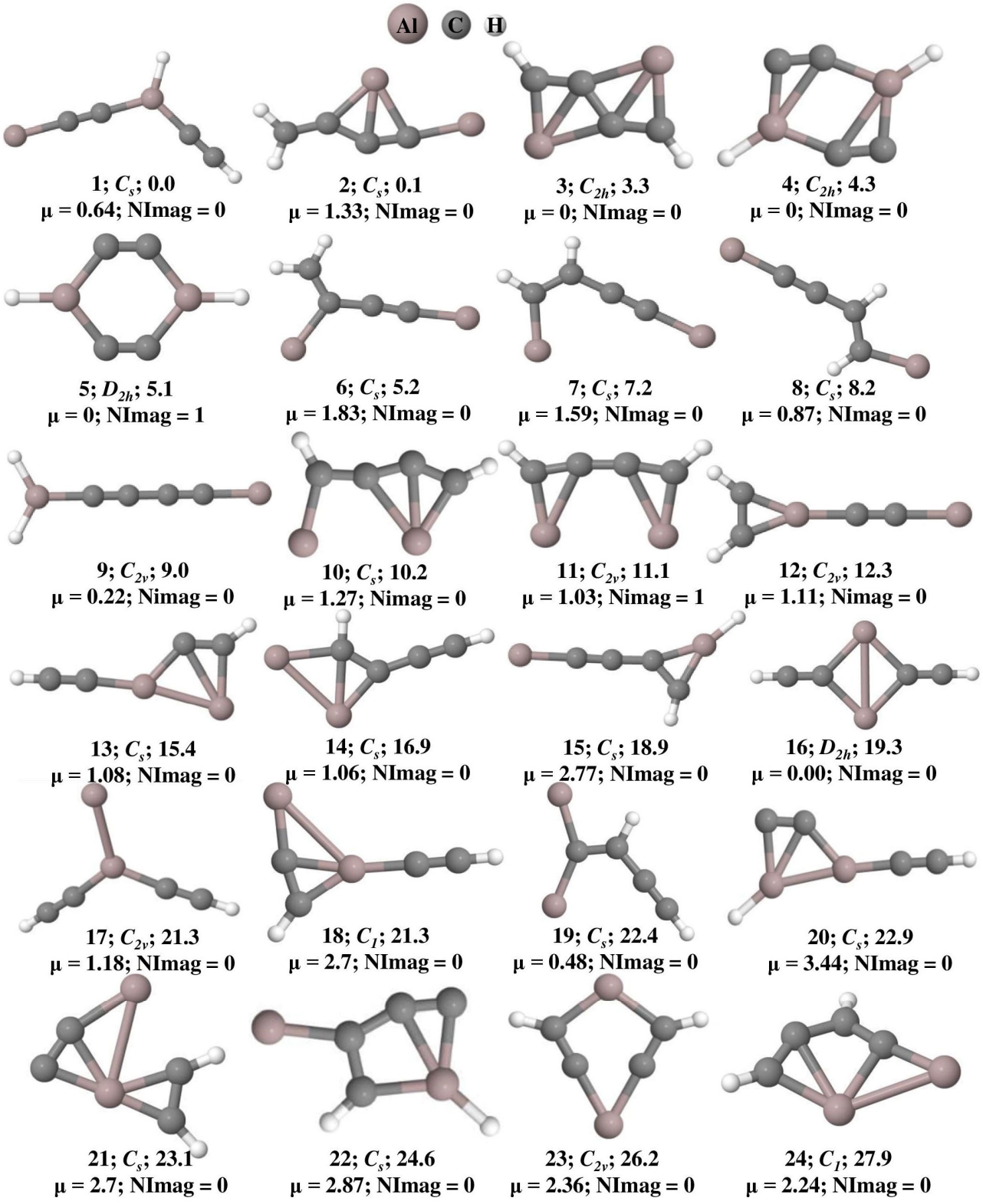

Figure 1. *Cont.*

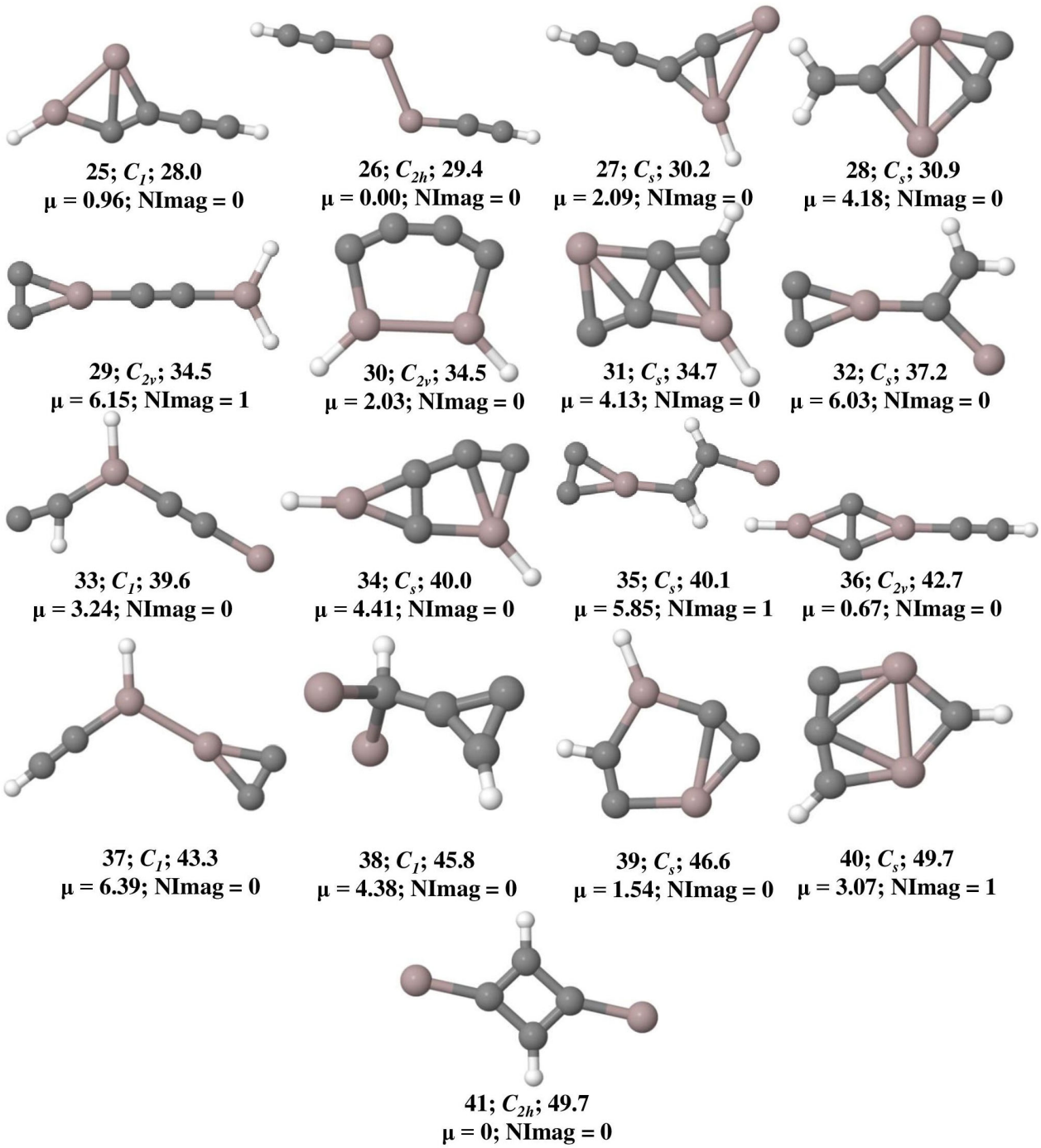

Figure 1. Isomers of $Al_2C_4H_2$ that lie within 50 kcal mol^{-1} and their zero-point vibrational energy (ZPVE) corrected relative energies (in kcal mol^{-1}), dipole moments (in Debye), and the number of imaginary frequencies (NImag) obtained at the ωB97XD/6-311++G(2d,2p) level of theory.

3.2. Topological Analysis

The electron localization function (ELF) analysis was carried out to measure the extent of electron delocalization in molecular systems. The color-filled ELF plots of isomers **3**, **4**, **14**, **18**, **20**, **21**, **22**, **28**, **31**, **34**, and **40** are shown in Figure 4. In isomer **3**, the electron density is localized between the ptC–C bonds in the range of 0.80 to 1.00 which indicates strong localization of electrons, and also the electron density is delocalized through the ptC–C bonds, contributing to its stability. Furthermore, both of the aluminum atoms are involved in the delocalization of electrons, which enhances the stability of isomer **3**. In isomers **14**,

22, **31**, and **34**, the electron density is delocalized along the C–C bonds, contributing to their structural stability. In the case of isomers **4**, **20**, **22**, **31**, and **34**, aluminum-attached hydrogen has electronegative values in the range of −0.345 to −0.378 $|e|$ as listed in Table S3 due to the high electropositive nature of aluminum compared to carbon. The Al–Al bonds in isomers **21**, **28**, and **40** have ELF values in the range of 0.00 to 0.50 which indicates the poor localization of electrons between these atoms.

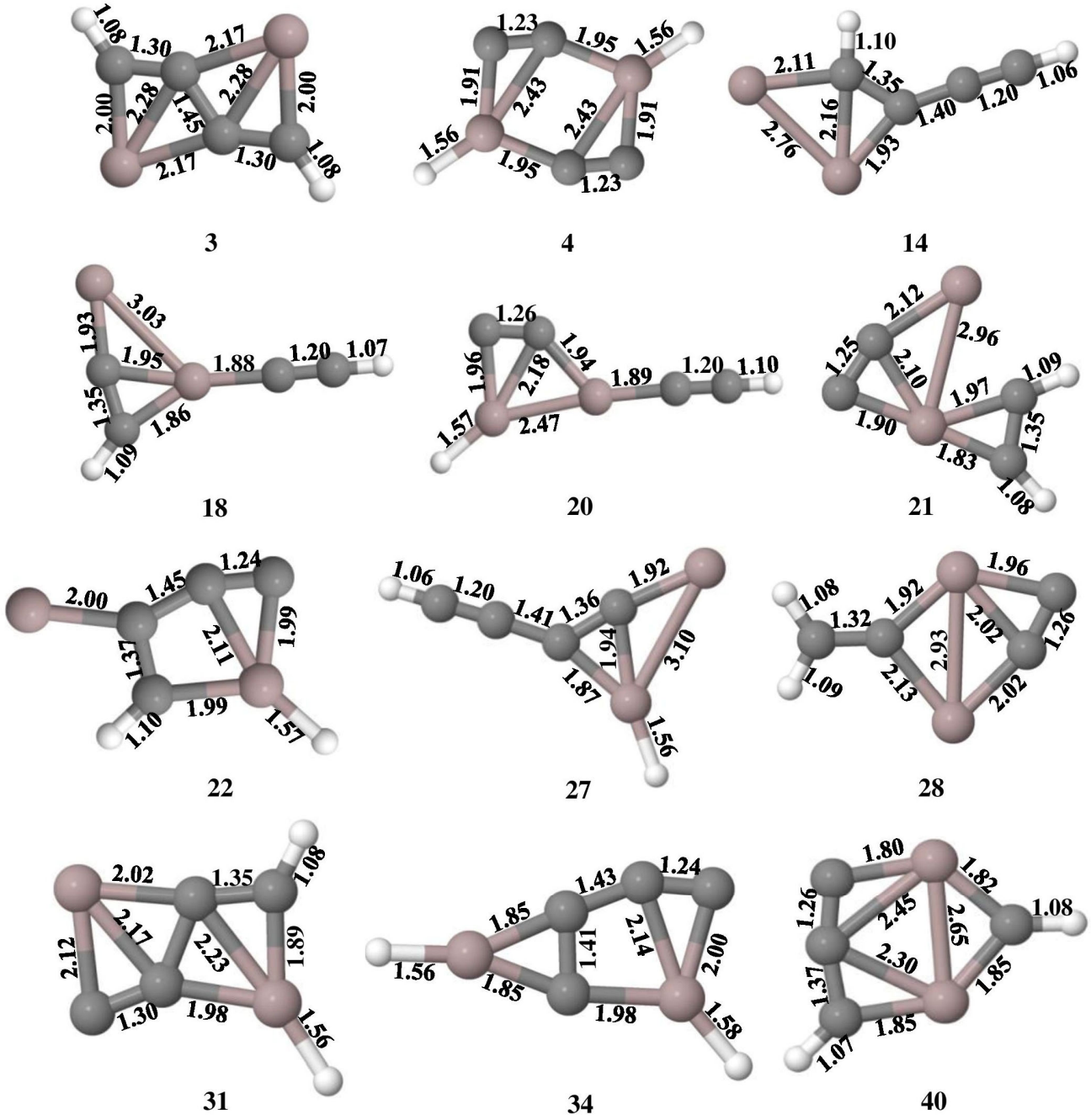

Figure 2. Isomers of $Al_2C_4H_2$ with the planar tetracoordinate carbon (ptC)/aluminum (ptAl) and planar pentacoordinate aluminum (ppAl) with their bond lengths in Å obtained at the ωB97XD/6-311++G(2d,2p) level of theory.

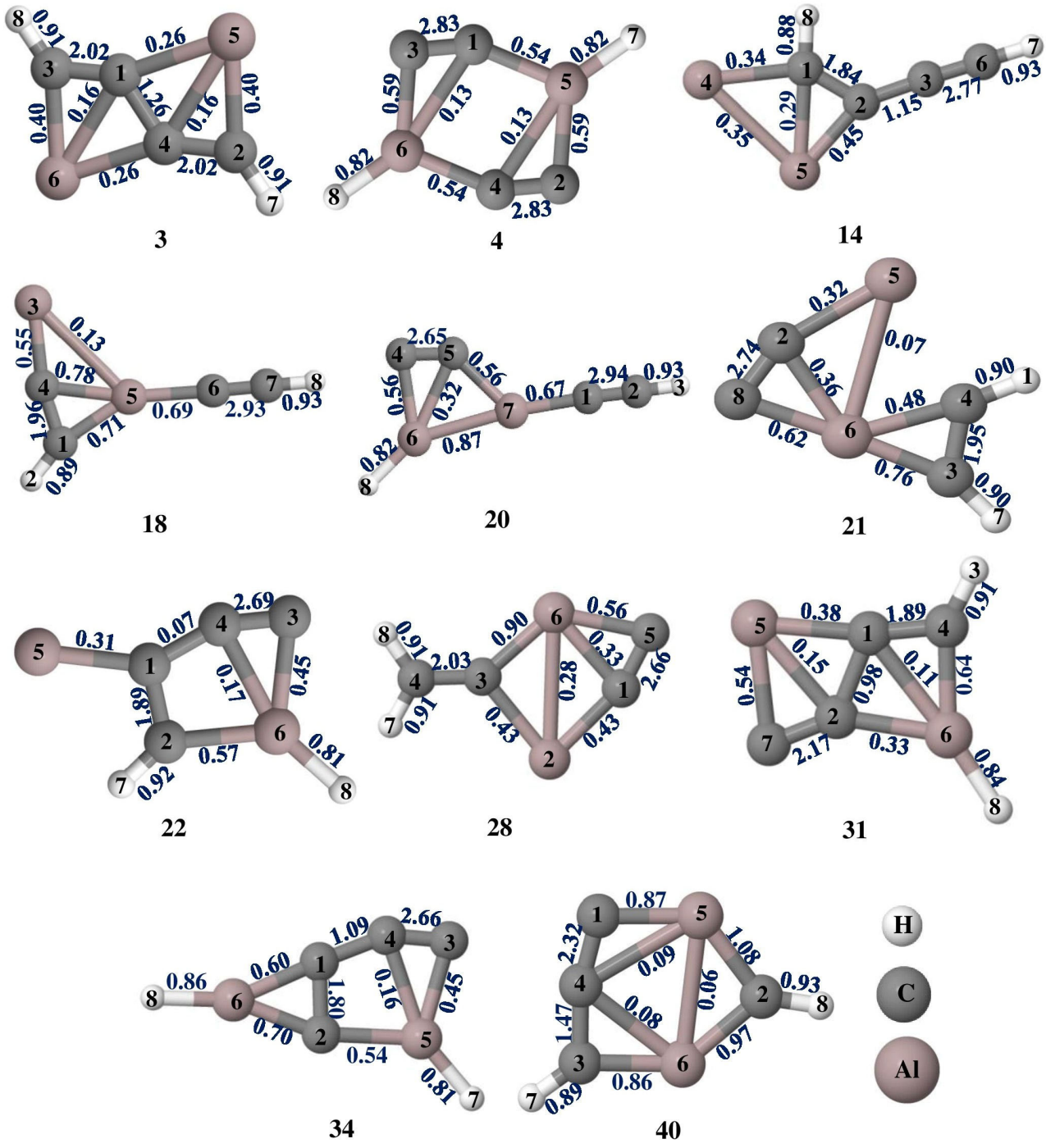

Figure 3. Wiberg bond indices of $Al_2C_4H_2$ isomers **3**, **4**, **14**, **18**, **20**, **21**, **22**, **28**, **31**, **34**, and **40** at the ωB97XD/6-311++G(2d,2p) level of theory.

3.3. Kinetic Stability

To explore the kinetic stability of ptC and ptAl isomers in the $Al_2C_4H_2$ system, ab initio molecular dynamics simulations were carried out using the ADMP approach. This study enables us to explore the structural variation through the atomic arrangement in the elemental composition. Isomers **3**, **4**, **14**, **18**, **20**, **21**, **22**, **28**, **31**, **34**, and **40** were considered for these simulations at 298 K and 1 atm pressure, and the simulations were carried out for up to 1000 fs. The structural stability in the time evolution of total energy for these isomers is given in Figure 5. The oscillations in the energy plots result from an increase in

nuclear kinetic energy during the structural deformation of the systems throughout the simulation. These plots demonstrate well-balanced energy oscillations for isomers **3**, **4**, **14**, **18**, **20**, **22**, **31**, **34**, and **40**. These isomers' structural stability is well retained throughout the simulated time scale, and no isomerization or other structural modifications take place in these molecules and they are kinetically stable except for isomer **21**. In the case of isomer **21**, the geometry deforms by entirely shattering the geometry and isomerizing it into the low-energy isomer **12**, confirming that it is kinetically unstable.

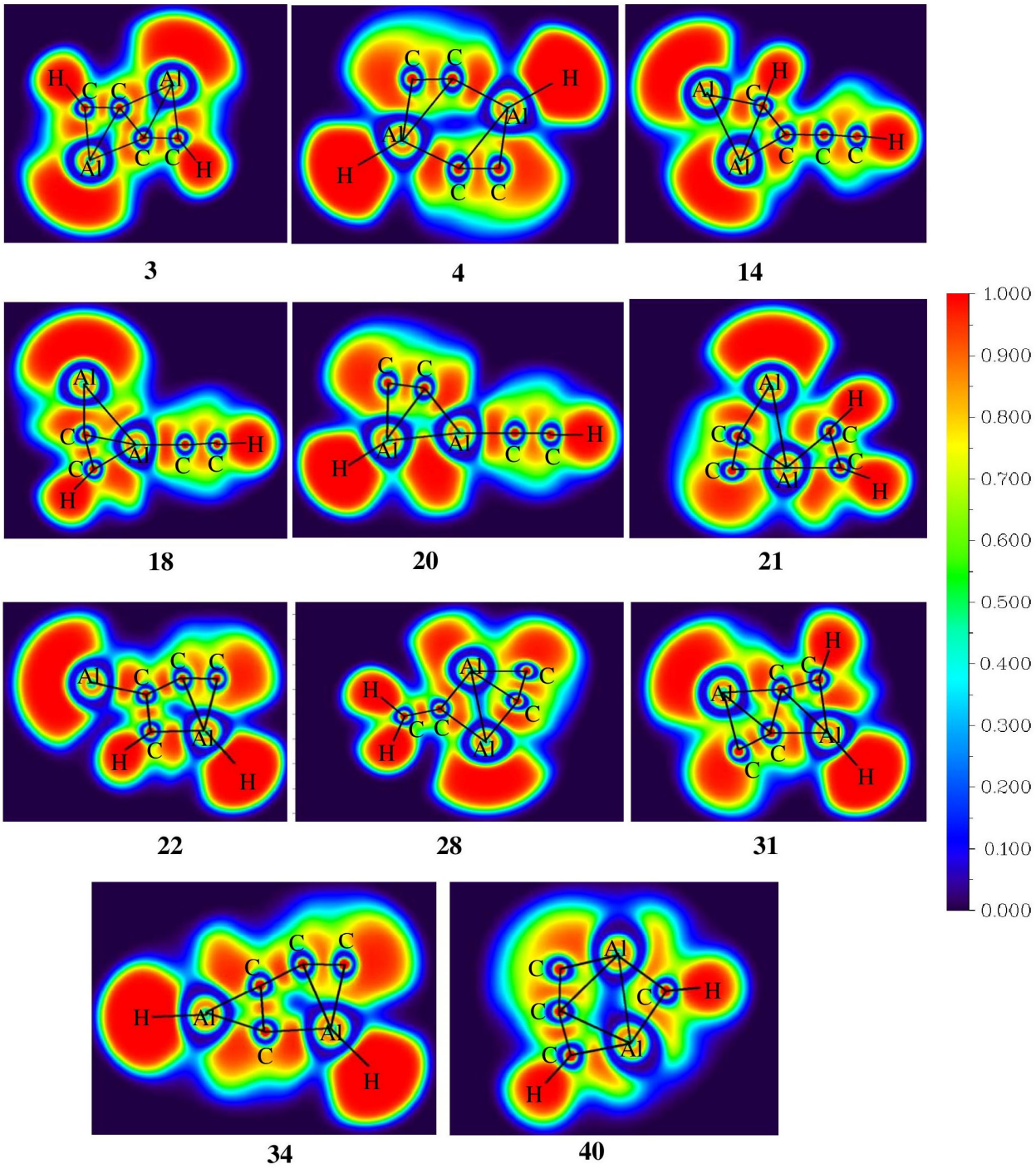

Figure 4. Color-filled map of ELF for isomers **3**, **4**, **14**, **18**, **20**, **21**, **22**, **28**, **31**, **34**, and **40** obtained at the ωB97XD/6-311++G(2d,2p) level of theory.

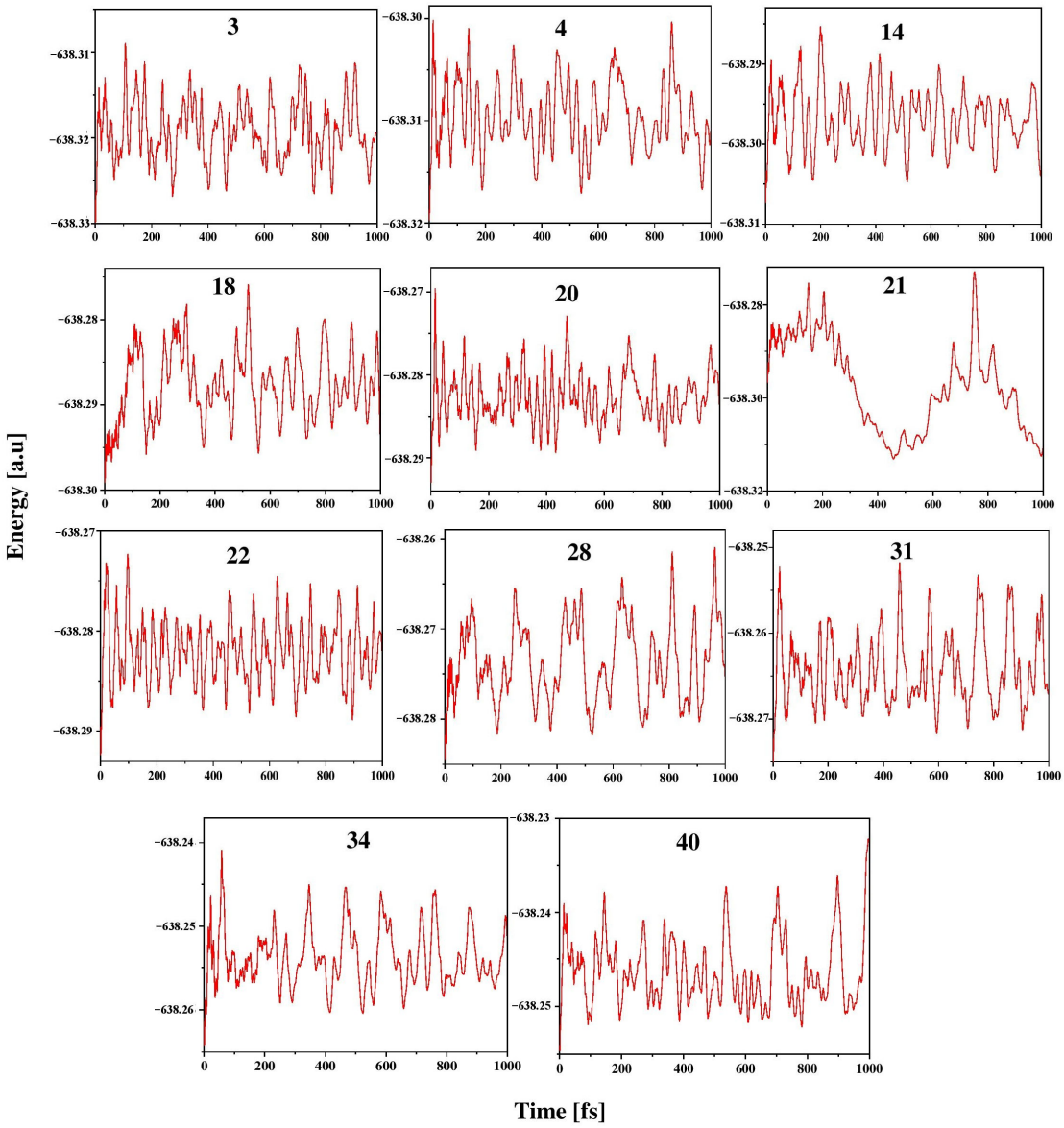

Figure 5. Energy evolution of isomers **3**, **4**, **14**, **18**, **20**, **21**, **22**, **28**, **31**, **34**, and **40** at 298 K, 1 atm pressure for 1000 fs of time in the ADMP simulation performed at the ωB97XD/6311++G(2d,2p) level.

3.4. Adaptive Natural Density Partitioning and Natural Bond Order Analysis

The adaptive natural density partitioning (AdNDP) analysis was performed for isomers **3**, **4**, **14**, **18**, **20**, **21**, **22**, **28**, **31**, **34**, and **40** which are illustrated in Figure 6 for multi-center–2e bonds and Figure S2 for lone pairs and 2c–2e bonds. It gives insight into delocalized multi-center–2e bonds as well as Lewis bonding components. In a Lewis structure, the good electron pair should have an occupancy number (ON) greater than 1.90 $|e|$. The 2c–2e σ bonds in all of the isomers have an ON value above 1.90 $|e|$ that dictates the electron density which is localized between the planar tetracoordinate centers and their adjacent atoms. The presence of multi-center–2e π bonds in isomers **3**, **14**, **22**, **31**, **34**, and **40** shows how the electrons participate in delocalization along C-C carbon bonds. In isomer **3**, four 3c–2e σ bonds with ON 1.99 and 1.98 $|e|$, two 3c–2e π bonds with ON 1.93 $|e|$, 4c–2e π bonds with ON 2.00 $|e|$, and a 5c–2e π bond with ON 1.99 $|e|$ are observed and are in accord with the concept of double aromaticity in the molecule as shown by the negative values of NICS (0) and NICS (1) in Figure S3. Delocalization encompasses the whole system, making isomer **3** more stable than other isomers. All the other isomers also have multi-center–2e bonds with ON greater than 1.90 $|e|$. In isomer **3**, the aluminum LP

orbitals with low ON 1.80 $|e|$, as shown in Figure S2, confirm that the electrons are shared by aluminum atoms which is consistent with NBO and ELF analysis.

The energies of donor–acceptor interaction of lone pairs of aluminum obtained for isomers **3**, **4**, **18**, **21**, **22**, **28**, and **31** with NBO analysis are presented in Table S4. The occupancies of lone pairs for isomers **3**, **14**, **18**, **21**, **22**, **28**, **31**, and **40** from NBO analysis are given in Table S5. The $E^{(2)}$ is the hyperconjugative interaction between acceptor and donor which governs the stabilization energy. The LP(Al5) → π*(C1–C4) and LP(Al6) → π*(C1–C4) in isomer **3** have larger stabilization energy of 36.71 kcal mol^{-1}, as compared to other isomers, which confirms that the electrons from both of the aluminum atoms are shared and accepted by surrounding atoms that is consistent with the delocalization nature of the structure obtained from ELF analysis.

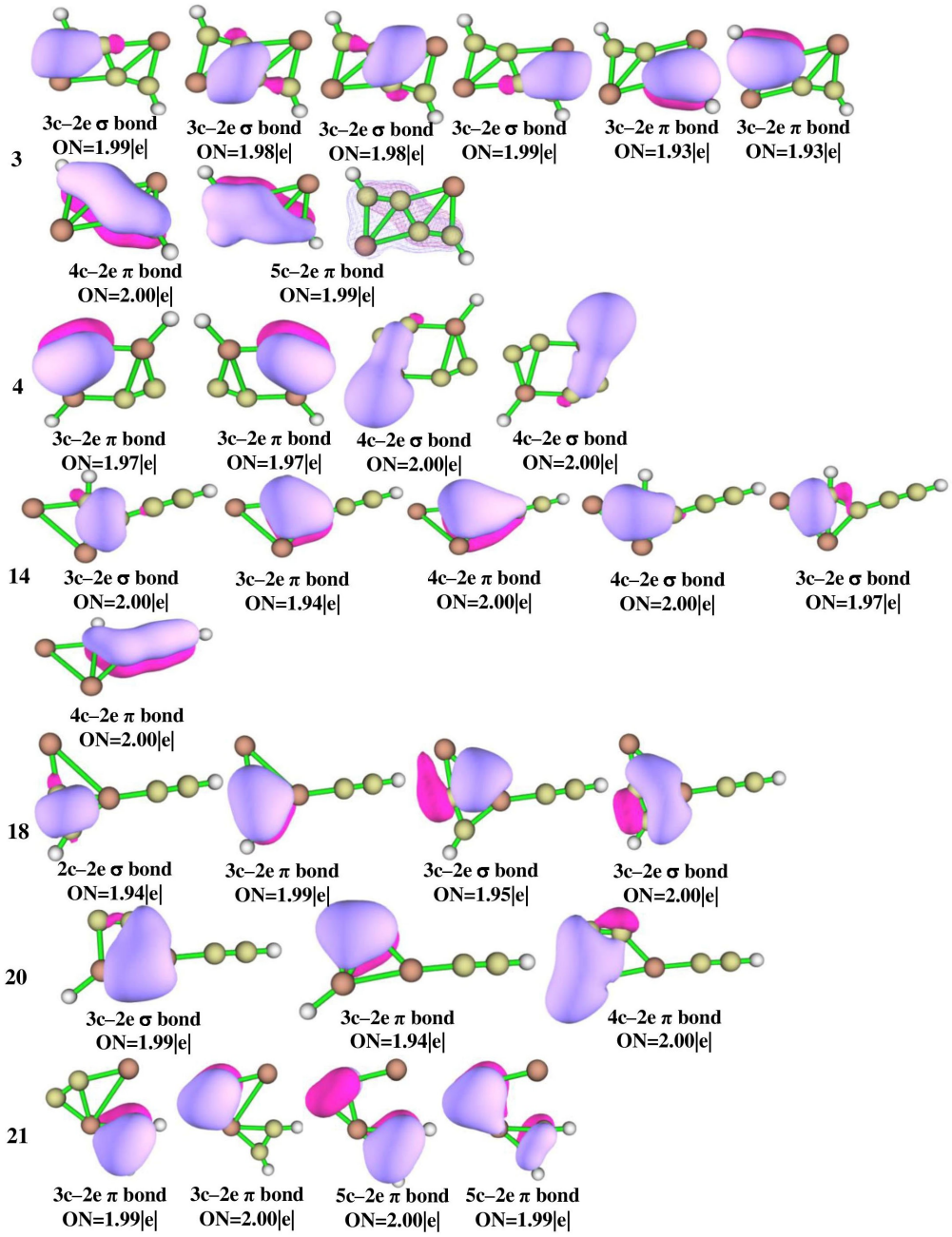

Figure 6. *Cont.*

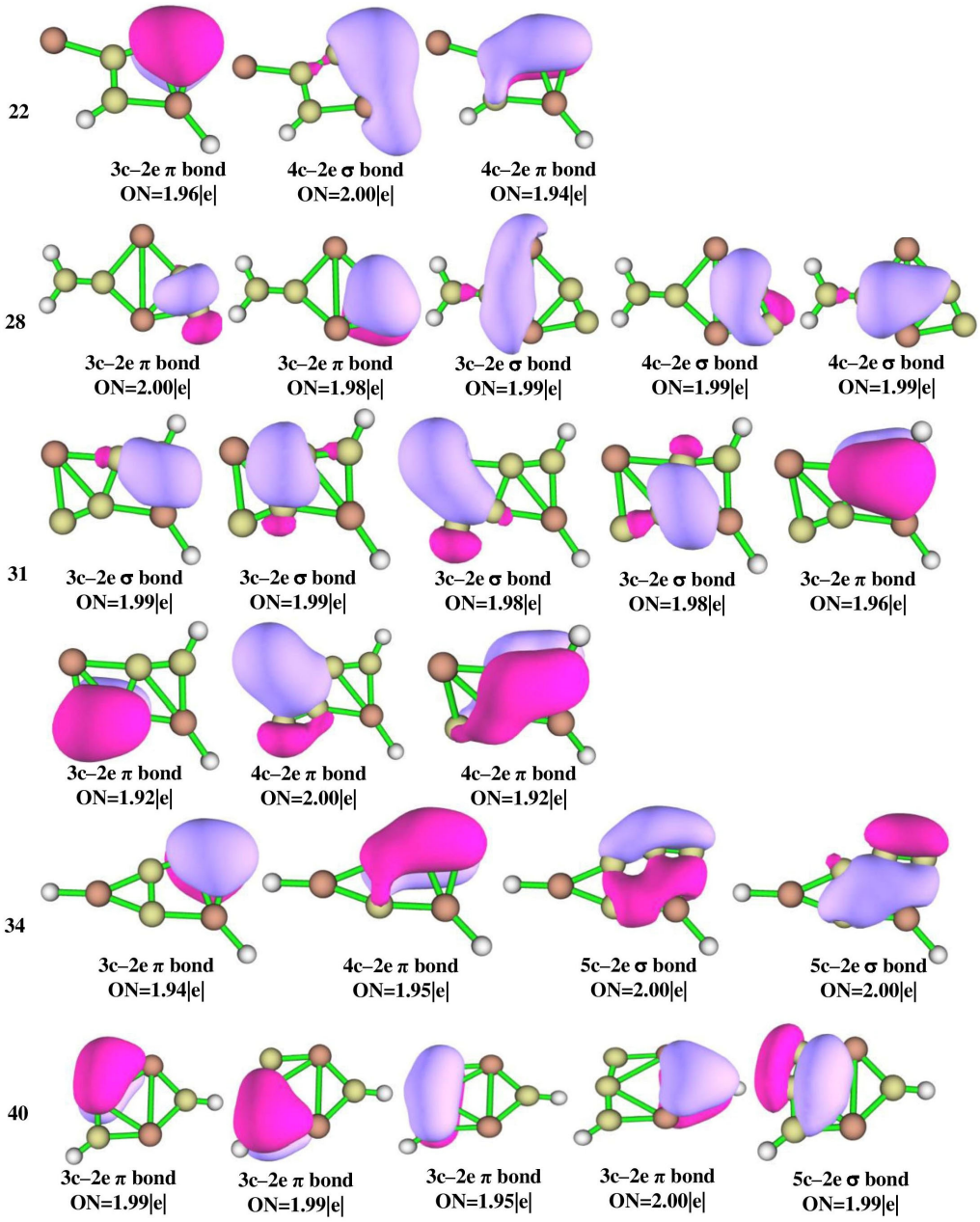

Figure 6. AdNDP bonding patterns of $Al_2C_4H_2$ isomers **3**, **4**, **14**, **18**, **20**, **21**, **22**, **28**, **31**, **34**, and **40** at the ωB97XD/6-311++G(2d,2p) level of theory.

4. Conclusions

In summary, the isomers of $Al_2C_4H_2$ have been explored at the ωB97XD/6-311++G(2d,2p) level of theory. The isomers containing planar tetracoordinate carbon/aluminum that lie within 50 kcal mol^{-1} are subjected to chemical bonding analysis. Isomers **3** and **4** are planar tetracoordinate systems that are energetically close to global minimum geometry **1**. The isomers that have the ptCs are energetically more stable than the isomers that contain ptAl because of the electron delocalization nature of ptC compared to ptAl. The isomers with ptC have one π bond and four σ bonds, while the isomers with ptAl have only four sigma bonds. Among the planar tetracoordinate isomers, isomer **3** is energetically stable due to its high delocalization nature and double aromaticity as observed in the ELF, NICS, and AdNDP analysis. So, the stability of isomer **3** is achieved by the tendency of the electron-donating nature of the aluminum atom. The ab initio molecular dynamics simulations revealed that all these planar tetracoordinate molecules are kinetically stable except isomer

21 which isomerizes to isomer **12**. Exploring the electron density distribution and orbital orientation of these isomers provides insight into the nature of chemical bonding and may lead to potential applications in the future. The insights of this work would impart great interest to experimentalists to find $Al_2C_4H_2$ isomers in the laboratory which remain elusive to date.

Supplementary Materials: The following supporting information can be downloaded at: https://www.mdpi.com/article/10.3390/atoms10040112/s1. The optimized geometries of all the isomers are given in Figure S1, AdNDP for lone pairs and 2c–2e bonds of isomers **3**, **4**, **14**, **18**, **20**, **21**, **22**, **28**, **31**, **34**, and **40** are given in Figure S2, NICS for isomer **3** is given in Figure S3, total energies (in a.u), zero-point vibrational energies (ZPVEs; in a.u.), ZPVE corrected total energies (E+ZPVE; in a.u.), relative energies (ΔE+ZPVE; in kcal mol^{-1}), and the number of imaginary frequencies (NImag) of $Al_2C_4H_2$ isomers calculated at ωB97XD/6-311++G(2d,2p) and B3LYP/6-311++G(2d,2p) level are given in Tables S1 and S2, respectively, natural atomic charges of hydrogen in isomers **3**, **4**, **14**, **18**, **20**, **21**, **22**, **28**, **31**, **34**, **and 40** are given in Table S3, the donor → acceptor orbitals of lone pairs of aluminum in isomers **3**, **4**, **18**, **21**, **22**, **28**, and **31** are given in **Table S4**, occupancies of lone pairs for isomers **3**, **14**, **18**, **21**, **22**, **28**, **31**, and **40** from NBO analysis are given in Table S5, cartesian coordinates of all isomers at ωB97XD/6-311++G(2d,2p) and B3LYP/6-311++G(2d,2p) level are given in Tables S6 and S7.

Author Contributions: Conceptualization, V.S.T. and K.T.; Investigation, A.H.M., S.S. (Sony Sobinson), N.J., S.S. (Shilpa Shajan), S.P.M., V.S.T. and K.T.; Methodology, A.H.M., S.S. (Sony Sobinson), N.J., S.S. (Shilpa Shajan), S.P.M., V.S.T. and K.T.; Supervision, V.S.T. and K.T.; Visualization, A.H.M., N.J., S.S. (Shilpa Shajan), S.P.M. and K.T.; Writing – original draft, A.H.M.; Writing – review & editing, V.S.T. and K.T. All authors have read and agreed to the published version of the manuscript.

Funding: This research work did not receive any specific grant from funding agencies in the public, commercial, or not-for-profit sectors.

Institutional Review Board Statement: Not applicable.

Informed Consent Statement: Not applicable.

Data Availability Statement: Data are available in the article or Supplementary Materials.

Acknowledgments: The computational facility provided at the VIT, Vellore, to carry out this work is gratefully acknowledged. Computational support provided at the SDSU (for VST) by DURIP Grant W911NF-10-1-0157 from the U.S. Department of Defense and by NSF CRIF Grant CHE-0947087 is gratefully acknowledged.

Conflicts of Interest: The authors declare no conflict of interest.

Abbreviations

The following abbreviations are used in this manuscript:

AdNDP	Adaptive Natural Density Partitioning
ADMP	Atom-centered Density Matrix Propagation
DFT	Density Functional Theory
ELF	Electron Localization Function
NBO	Natural Bond Order
ON	Occupation Number
ptC	Planar Tetracoordinate Carbon
phC	Planar Hypercoordinate Carbon
ptAl	Planar Tetracoordinate Aluminum
ppAl	Planar Pentacoordinate Aluminum
WBI	Wiberg Bond Index
LP	Lone Pair

References

1. Leyva-Parra, L.; Inostroza, D.; Yañez, O.; Cruz, J.C.; Garza, J.; García, V.; Tiznado, W. Persistent Planar Tetracoordinate Carbon in Global Minima Structures of Silicon-Carbon Clusters. *Atoms* **2022**, *10*, 27. [CrossRef]
2. Das, P.; Khatun, M.; Anoop, A.; Chattaraj, P.K. $CSi_nGe_{4-n}^{2+}$ (n = 1–3): Prospective Systems Containing Planar Tetracoordinate Carbon (PtC). *Phys. Chem. Chem. Phys.* **2022**, *24*, 16701–16711. [CrossRef]
3. Yañez, O.; Vásquez-Espinal, A.; Báez-Grez, R.; Rabanal-León, W.A.; Osorio, E.; Ruiz, L.; Tiznado, W. Carbon Rings Decorated with Group 14 Elements: New Aromatic Clusters Containing Planar Tetracoordinate Carbon. *New J. Chem.* **2019**, *43*, 6781–6785. [CrossRef]
4. Yang, L.M.; Ganz, E.; Chen, Z.; Wang, Z.X.; Schleyer, P.V.R. Four Decades of the Chemistry of Planar Hypercoordinate Compounds. *Angew. Chem.-Int. Ed.* **2015**, *54*, 9468–9501. [CrossRef]
5. Merino, G.; Méndez-Rojas, M.A.; Beltrán, H.I.; Corminboeuf, C.; Heine, T.; Vela, A. Theoretical Analysis of the Smallest Carbon Cluster Containing a Planar Tetracoordinate Carbon. *J. Am. Chem. Soc.* **2004**, *126*, 16160–16169. [CrossRef]
6. Pancharatna, P.D.; Méndez-Rojas, M.A.; Merino, G.; Vela, A.; Hoffmann, R. Planar Tetracoordinate Carbon in Extended Systems. *J. Am. Chem. Soc.* **2004**, *126*, 15309–15315. [CrossRef]
7. Zhao, J.; Liu, B.; Zhai, H.; Zhou, R.; Ni, G.; Xu, Z. Mass Spectrometric and First Principles Study of Al_nC^- Clusters. *Solid State Commun.* **2002**, *122*, 543–547. [CrossRef]
8. Jensen, C.M.; Gross, K.J. Development of Catalytically Enhanced Sodium Aluminum Hydride as a Hydrogen-Storage Material. *Appl. Phys. A Mater. Sci. Process.* **2001**, *72*, 213–219. [CrossRef]
9. Leskiw, B.D.; Castleman, A.W. The Interplay between the Electronic Structure and Reactivity of Aluminum Clusters: Model Systems as Building Blocks for Cluster Assembled Materials. *Chem. Phys. Lett.* **2000**, *316*, 31–36. [CrossRef]
10. Suresh, C.H.; Frenking, G. Direct 1−3 Metal−Carbon Bonding and Planar Tetracoordinated Carbon in Group 6 Metallacyclobutadienes. *Organometallics* **2010**, *29*, 4766–4769. [CrossRef]
11. Ghana, P.; Rump, J.; Schnakenburg, G.; Arz, M.I.; Filippou, A.C. Planar Tetracoordinated Silicon (PtSi): Room-Temperature Stable Compounds Containing Anti-van't Hoff/Le Bel Silicon. *J. Am. Chem. Soc.* **2021**, *143*, 420–432. [CrossRef]
12. Ebner, F.; Greb, L. Calix [4]Pyrrole Hydridosilicate: The Elusive Planar Tetracoordinate Silicon Imparts Striking Stability to Its Anionic Silicon Hydride. *J. Am. Chem. Soc.* **2018**, *140*, 17409–17412. [CrossRef] [PubMed]
13. Xu, J.; Zhang, X.; Yu, S.; Ding, Y.H.; Bowen, K.H. Identifying the Hydrogenated Planar Tetracoordinate Carbon: A Combined Experimental and Theoretical Study of CAl_4H and CAl_4H^-. *J. Phys. Chem. Lett.* **2017**, *8*, 2263–2267. [CrossRef]
14. Keese, R. Carbon Flatland: Planar Tetracoordinate Carbon and Fenestranes. *Chem. Rev.* **2006**, *106*, 4787–4808. [CrossRef]
15. Li, X.; Zhang, H.-F.; Wang, L.-S.; Geske, G.D.; Boldyrev, A.I. Pentaatomic Tetracoordinate Planar Carbon, $[CAl_4]^{2-}$: A New Structural Unit and Its Salt Complexes. *Angew. Chem.* **2000**, *39*, 3630–3632. [CrossRef]
16. Li, X.; Wang, L.S.; Boldyrev, A.I.; Simons, J. Tetracoordinated Planar Carbon in the Al_4C^- Anion. A Combined Photoelectron Spectroscopy and Ab Initio Study. *J. Am. Chem. Soc.* **1999**, *121*, 6033–6038. [CrossRef]
17. Boldyrev, A.I.; Simons, J. Tetracoordinated Planar Carbon in Pentaatomic Molecules. *J. Am. Chem. Soc.* **1998**, *120*, 7967–7972. [CrossRef]
18. Erker, G. Planar-Tetracoordinate Carbon: Making Stable Anti-van't Hoff/LeBel Compounds. *Comments Inorg. Chem.* **1992**, *13*, 111–131. [CrossRef]
19. Cotton, F.A.; Millar, M. The Probable Existence of a Triple Bond between Two Vanadium Atoms. *J. Am. Chem. Soc.* **1977**, *99*, 7886–7891. [CrossRef]
20. Röttger, D.; Erker, G. Compounds Containing Planar-Tetracoordinate Carbon. *Angew. Chem. Int. Ed. Eng.* **1997**, *36*, 812–827. [CrossRef]
21. Van't Hoff, J.H. A Suggestion Looking To the Extension Into Space of the Structural Formulas At Present Used in Chemistry. and a Note Upon the Relation Between the Optical Activity and the Chemical Constitution of Organic Compounds. *Arch. Neerl. Des Sci. Exactes Nat.* **1874**, *9*, 445–454.
22. Le Bel, J.A. On the Relations Which Exist between the Atomic Formulas of Organic Compounds and the Rotatory Power of Their Solutions. *Bull. Soc. Chim. Fr.* **1874**, *22*, 337–347.
23. Vassilev-Galindo, V.; Pan, S.; Donald, K.J.; Merino, G. Planar Pentacoordinate Carbons. *Nat. Rev. Chem.* **2018**, *2*, 0114. [CrossRef]
24. Monkhorst, J.H. Activation Energy for Interconversion of enantiomers containing an asymmetric carbon atom without breaking bonds. *Chem. Commun.* **1968**, 1111–1112. [CrossRef]
25. Hoffmann, R.; Alder, R.W.; Wilcox, C.F. Planar Tetracoordinate Carbon. *J. Am. Chem. Soc.* **1970**, *92*, 4992–4993. [CrossRef]
26. Collins, J.B.; Dill, J.D.; Jemmis, E.D.; Apeloig, Y.; Schleyer, P.V.R.; Collins, J.B.; Jemmis, E.D.; Schleyer, P.V.R.; Seeger, R.; Pople, J.A. Stabilization of Planar Tetracoordinate Carbon. *J. Am. Chem. Soc.* **1976**, *98*, 5419–5427. [CrossRef]
27. Pei, Y.; An, W.; Ito, K.; Schleyer, P.V.R.; Xiao, C.Z. Planar Pentacoordinate Carbon in CAI_5^+: A Global Minimum. *J. Am. Chem. Soc.* **2008**, *130*, 10394–10400. [CrossRef]
28. Li, Y.; Liao, Y.; Schleyer, P.V.R.; Chen, Z. Al_2C Monolayer: The Planar Tetracoordinate Carbon Global Minimum. *Nanoscale* **2014**, *6*, 10784–10791. [CrossRef] [PubMed]
29. Li, Y.; Liao, Y.; Chen, Z. Be_2C Monolayer with Quasi-Planar Hexacoordinate Carbons: A Global Minimum Structure. *Angew. Chem.-Int. Ed.* **2014**, *53*, 7248–7252. [CrossRef]

30. Zhang, Z.; Liu, X.; Yakobson, B.I.; Guo, W. Two-Dimensional Tetragonal TiC Monolayer Sheet and Nanoribbons. *J. Am. Chem. Soc.* **2012**, *134*, 19326–19329. [CrossRef]
31. Wu, X.; Pei, Y.; Zeng, X.C. B_2C Graphene, Nanotubes, and Nanoribbons. *Nano Lett.* **2009**, *9*, 1577–1582. [CrossRef] [PubMed]
32. Wang, Y.; Li, F.; Li, Y.; Chen, Z. Semi-Metallic Be_5C_2 Monolayer Global Minimum with Quasi-Planar Pentacoordinate Carbons and Negative Poisson's Ratio. *Nat. Commun.* **2016**, *7*, 11488. [CrossRef]
33. Wang, L.-S.; Boldyrev, A.I.; Li, X.; Simons, J. Experimental Observation of Pentaatomic Tetracoordinate Planar Carbon-Containing Molecules. *J. Am. Chem. Soc.* **2000**, *122*, 7681–7687. [CrossRef]
34. Zhai, H.J.; Wang, L.S.; Alexandrova, A.N.; Boldyrev, A.I. Electronic Structure and Chemical Bonding of B_5^- and B_5 by Photoelectron Spectroscopy and Ab Initio Calculations. *J. Chem. Phys.* **2002**, *117*, 7917–7924. [CrossRef]
35. Wang, L.M.; Huang, W.; Averkiev, B.B.; Boldyrev, A.I.; Wang, L.S. CB_7^-: Experimental and Theoretical Evidence against Hypercoordinate Planar Carbon. *Angew. Chem.-Int. Ed.* **2007**, *46*, 4550–4553. [CrossRef]
36. Averkiev, B.B.; Zubarev, D.Y.; Wang, L.M.; Huang, W.; Wang, L.S.; Boldyrev, A.I. Carbon Avoids Hypercoordination in CB_6^-, CB_6^{2-}, and $C_2B_5^-$ Planar Carbon-Boron Clusters. *J. Am. Chem. Soc.* **2008**, *130*, 9248–9250. [CrossRef]
37. Dong, F.; Heinbuch, S.; Xie, Y.; Rocca, J.J.; Bernstein, E.R. Experimental and Theoretical Study of Neutral Al_mC_n and $Al_mC_nH_x$ Clusters. *Phys. Chem. Chem. Phys.* **2010**, *12*, 2569–2581. [CrossRef]
38. Sergeeva, A.P.; Piazza, Z.A.; Romanescu, C.; Li, W.L.; Boldyrev, A.I.; Wang, L.S. B_{22}^- and B_{23}^-: All-Boron Analogues of Anthracene and Phenanthrene. *J. Am. Chem. Soc.* **2012**, *134*, 18065–18073. [CrossRef]
39. Zhang, C.-J.; Wang, P.; Xu, X.-L.; Xu, H.-G.; Zheng, W.-J. Photoelectron Spectroscopy and Theoretical Study of $Al_nC_5^{-/0}$ (n = 1–5) Clusters: Structural Evolution, Relative Stability of Star-like Clusters, and Planar Tetracoordinate Carbon Structures. *Phys. Chem. Chem. Phys.* **2021**, *23*, 1967–1975. [CrossRef]
40. Wu, Y.-B.; Lu, H.-G.; Li, S.-D.; Wang, Z.-X. Simplest Neutral Singlet C_2E_4 (E = Al, Ga, In, and Tl) Global Minima with Double Planar Tetracoordinate Carbons: Equivalence of C_2 Moieties in C_2E_4 to Carbon Centers in CAl_4^{2-} and CAl_5^+. *J. Phys. Chem. A* **2009**, *113*, 3395–3402. [CrossRef]
41. Wu, Y.B.; Jiang, J.L.; Lu, H.G.; Wang, Z.X.; Perez-Peralta, N.; Islas, R.; Contreras, M.; Merino, G.; Wu, J.I.C.; Von Ragué Schleyer, P. Starlike Aluminum-Carbon Aromatic Species. *Chem. Eur. J.* **2011**, *17*, 714–719. [CrossRef] [PubMed]
42. Xie, H.B.; Ding, Y.H. C Al_4 X (X=Si,Ge): Molecules with Simultaneous Planar Tetracoordinate Carbon, Aluminum, and Silicon/Germanium. *J. Chem. Phys.* **2007**, *126*, 184302. [CrossRef] [PubMed]
43. Irving, B.J.; Naumkin, F.Y. Communication: A Density Functional Investigation of Structure-Property Evolution in the Tetrakis Hexahedral C_4Al_{14} Nanocluster. *J. Chem. Phys.* **2014**, *141*, 131102. [CrossRef] [PubMed]
44. Boldyrev, A.I.; Simons, J.; Li, X.; Wang, L. Photoelectron Spectroscopy and Ab Initio Study. *J. Am. Chem. Soc.* **1999**, *121*, 10193–10197. [CrossRef]
45. Zhang, C.; Dai, W.; Xu, H.; Xu, X.; Zheng, W. Structural Evolution of Carbon-Doped Aluminum Clusters Al_nC^- (n = 6–15): Anion Photoelectron Spectroscopy and Theoretical Calculations. *J. Phys. Chem. A* **2022**, *126*, 5621–5631. [CrossRef] [PubMed]
46. Naumkin, F.Y. Flat-Structural Motives in Small Alumino−Carbon Clusters C_nAl_m (n = 2−3, m = 2−8). *J. Phys. Chem. A* **2008**, *112*, 4660–4668. [CrossRef]
47. Das, P.; Chattaraj, P.K. $CSiGaAl_2^{-/0}$ and $CGeGaAl_2^{-/0}$ Having Planar Tetracoordinate Carbon Atoms in Their Global Minimum Energy Structures. *J. Comput. Chem.* **2022**, *43*, 894–905. [CrossRef] [PubMed]
48. Maatallah, M.; Guo, M.; Cherqaoui, D.; Jarid, A.; Liebman, J.F. Aluminium Clusters for Molecular Hydrogen Storage and the Corresponding Alanes as Fuel Alternatives: A Structural and Energetic Analysis. *Int. J. Hydrogen Energy* **2013**, *38*, 5758–5767. [CrossRef]
49. Dai, J.; Wu, X.; Yang, J.; Zeng, X.C. Al_xC Monolayer Sheets: Two-Dimensional Networks with Planar Tetracoordinate Carbon and Potential Applications as Donor Materials in Solar Cell. *J. Phys. Chem. Lett.* **2014**, *5*, 2058–2065. [CrossRef]
50. Job, N.; Khatun, M.; Thirumoorthy, K.; CH, S.S.R.; Chandrasekaran, V.; Anoop, A.; Thimmakondu, V.S. $CAl_4Mg^{0/-}$: Global Minima with a Planar Tetracoordinate Carbon Atom. *Atoms* **2021**, *9*, 24. [CrossRef]
51. Khatun, M.; Roy, S.; Giri, S.; CH, S.S.R.; Anoop, A.; Thimmakondu, V.S. BAl4Mg$^{-/0/+}$: Global Minima with a Planar Tetracoordinate or Hypercoordinate Boron Atom. *Atoms* **2021**, *9*, 89. [CrossRef]
52. Georgakilas, V.; Tiwari, J.N.; Kemp, K.C.; Perman, J.A.; Bourlinos, A.B.; Kim, K.S.; Zboril, R. Noncovalent Functionalization of Graphene and Graphene Oxide for Energy Materials, Biosensing, Catalytic, and Biomedical Applications. *Chem. Rev.* **2016**, *116*, 5464–5519. [CrossRef]
53. A/RES/71/313. Available online: https://web.archive.org/web/20201128194012/https://undocs.org/A/RES/71/313 (accessed on 7 October 2022).
54. Tian, Y.H.; Hu, S.; Sheng, X.; Duan, Y.; Jakowski, J.; Sumpter, B.G.; Huang, J. Non-Transition-Metal Catalytic System for N_2 Reduction to NH_3: A Density Functional Theory Study of Al-Doped Graphene. *J. Phys. Chem. Lett.* **2018**, *9*, 570–576. [CrossRef] [PubMed]
55. Wang, R.; Zhang, D.; Sun, W.; Han, Z.; Liu, C. A Novel Aluminum-Doped Carbon Nanotubes Sensor for Carbon Monoxide. *J. Mol. Struct. THEOCHEM* **2007**, *806*, 93–97. [CrossRef]
56. Dai, J.; Yuan, J.; Giannozzi, P. Gas Adsorption on Graphene Doped with B, N, Al, and S: A Theoretical Study. *Appl. Phys. Lett.* **2009**, *95*, 232105. [CrossRef]

57. Compaan, K.R.; Agarwal, J.; Dye, B.E.; Yamaguchi, Y.; Schaefer, H.F. Toward Detection of $AlCH_2$ and $AlCH_2^+$ in the Interstellar Medium. *Astrophys. J.* **2013**, *778*, 125–130. [CrossRef]
58. Janczyk, A.; Ziurys, L.M. Laboratory Detection and Pure Rotational Spectrum of AlSH (X∼1A'). *Astrophys. J.* **2006**, *639*, L107–L110. [CrossRef]
59. Yousefi, M.; Bernath, P.F. Line Lists for AlF and AlCl in the X $^1\Sigma^+$ Ground State. *Astrophys. J. Suppl. Ser.* **2018**, *237*, 8. [CrossRef]
60. Hedderich, H.G.; Dulick, M.; Bernath, P.F. High Resolution Emission Spectroscopy of AlCl at 20 μ. *J. Chem. Phys.* **1993**, *99*, 8363–8370. [CrossRef]
61. Hoeft, J.; Lovas, F.J.; Tiemann, E.; Törring, T. Microwave Absorption Spectra of AlF, GaF, InF, and TIF. *Z. Naturforsch. A* **1970**, *25*, 1029–1035. [CrossRef]
62. Tenenbaum, E.D.; Ziurys, L.M. Exotic Metal Molecules in Oxygen-Rich Envelopes: Detection of AlOH (X $^1\Sigma^+$) in VY Canis Majoris. *Astrophys. J. Lett.* **2010**, *712*, 93–97. [CrossRef]
63. Walker, K.A.; Gerry, M.C. Laboratory Microwave Spectroscopy of Aluminium Cyanide. *Chem. Phys. Lett.* **1999**, *301*, 200–204. [CrossRef]
64. Ma, B.; Yamaguchi, Y.; Schaefer, H.F. Spectroscopic Constants and Potential Energy Surfaces for the Possible Interstellar Molecules A1NC and A1CN. *Mol. Phys.* **1995**, *86*, 1331–1337. [CrossRef]
65. Ziurys, L.M.; Savage, C.; Highberger, J.L.; Apponi, A.J.; Guélin, M.; Cernicharo, J. More Metal Cyanide Species: Detection of AlNC (X $^1\Sigma^+$) toward IRC +10216. *Astrophys. J.* **2002**, *564*, L45–L48. [CrossRef]
66. Tenenbaum, E.D.; Ziurys, L.M. Millimeter Detection of Alo (X $^2\Sigma^+$): Metal Oxide Chemistry in the Envelope of VY Canis Majoris. *Astrophys. J.* **2009**, *694*, 59–63. [CrossRef]
67. Kamiński, T.; Müller, H.S.P.; Schmidt, M.R.; Cherchneff, I.; Wong, K.T.; Brünken, S.; Menten, K.M.; Winters, J.M.; Gottlieb, C.A.; Patel, N.A. An Observational Study of Dust Nucleation in Mira (o Ceti). *Astron. Astrophys.* **2017**, *599*, A59. [CrossRef]
68. Gobrecht, D.; Plane, J.M.C.; Bromley, S.T.; Decin, L.; Cristallo, S.; Sekaran, S. Bottom-up Dust Nucleation Theory in Oxygen-Rich Evolved Stars I. Aluminium Oxide Clusters. *Astron. Astrophys.* **2021**, *658*, A167. [CrossRef]
69. Kramers, J.D.; Belyanin, G.A.; Przybyłowicz, W.J.; Winkler, H.; Andreoli, M.A.G. The Chemistry of the Extraterrestrial Carbonaceous Stone "Hypatia": A Perspective on Dust Heterogeneity in Interstellar Space. *Icarus* **2022**, *382*, 115043. [CrossRef]
70. Krishnan, R.; Binkley, J.S.; Seeger, R.; Pople, J.A. Self-consistent Molecular Orbital Methods. XX. A Basis Set for Correlated Wave Functions. *J. Chem. Phys.* **1980**, *72*, 650–654. [CrossRef]
71. Clark, T.; Chandrasekhar, J.; Spitznagel, G.W.; Schleyer, P.V.R. Efficient Diffuse Function-Augmented Basis Sets for Anion Calculations. III. The 3-21+G Basis Set for First-Row Elements, Li-F. *J. Comput. Chem.* **1983**, *4*, 294–301. [CrossRef]
72. Lee, C.; Yang, W.; Parr, R.G. Development of the Colle-Salvetti Correlation-Energy Formula into a Functional of the Electron Density. *Phys. Rev. B* **1988**, *37*, 785–789. [CrossRef] [PubMed]
73. Becke, A.D. Density-Functional Exchange-Energy Approximation with Correct Asymptotic Behavior. *Phys. Rev. A* **1988**, *38*, 3098–3100. [CrossRef] [PubMed]
74. Chai, J.-D.; Head-Gordon, M. Long-Range Corrected Hybrid Density Functionals with Damped Atom–Atom Dispersion Corrections. *Phys. Chem. Chem. Phys.* **2008**, *10*, 6615. [CrossRef]
75. Reed, A.E.; Weinstock, R.B.; Weinhold, F. Natural Population Analysis. *J. Chem. Phys.* **1985**, *83*, 735–746. [CrossRef]
76. Zubarev, D.Y.; Boldyrev, A.I. "Developing Paradigms of Chemical Bonding: Adaptive Natural Density Partitioning. *Phys. Chem. Chem. Phys.* **2008**, *10*, 5207. [CrossRef] [PubMed]
77. Zubarev, D.Y.; Boldyrev, A.I. Revealing Intuitively Assessable Chemical Bonding Patterns in Organic Aromatic Molecules via Adaptive Natural Density Partitioning. *J. Org. Chem.* **2008**, *73*, 9251–9258. [CrossRef] [PubMed]
78. Glendening, E.D.; Weinhold, F. Natural Resonance Theory: I. General Formalism. *J. Comput. Chem.* **1998**, *19*, 593–609. [CrossRef]
79. Von Ragué Schleyer, P.; Maerker, C.; Dransfeld, A.; Jiao, H.; van Eikema Hommes, N.J.R. Nucleus-Independent Chemical Shifts: A Simple and Efficient Aromaticity Probe. *J. Am. Chem. Soc.* **1996**, *118*, 6317–6318. [CrossRef]
80. Becke, A.D.; Edgecombe, K.E. A Simple Measure of Electron Localization in Atomic and Molecular Systems. *J. Chem. Phys.* **1990**, *92*, 5397–5403. [CrossRef]
81. Lu, T.; Chen, F. Multiwfn: A Multifunctional Wavefunction Analyzer. *J. Comput. Chem.* **2012**, *33*, 580–592. [CrossRef]
82. Schlegel, H.B.; Millam, J.M.; Iyengar, S.S.; Voth, G.A.; Daniels, A.D.; Scuseria, G.E.; Frisch, M.J. Ab Initio Molecular Dynamics: Propagating the Density Matrix with Gaussian Orbitals. *J. Chem. Phys.* **2001**, *114*, 9758–9763. [CrossRef]
83. Frisch, M.J.; Trucks, G.W.; Schlegel, H.B.; Scuseria, G.E.; Robb, M.A.; Cheeseman, J.R.; Scalmani, G.; Barone, V.; Petersson, G.A.; Nakatsuji, H.; et al. *Gaussian 16 Revision B.01*; Gaussian Inc.: Wallingford, CT, USA, 2016.